Check for updates

Characterization of steel billet scales generated during the continuous casting process in SIDERPERU steel plant

L. E. Borja-Castro[1] · A. Bustamante Dominguez[1] · M. I. Valerio-Cuadros[1,2] · R. A. Valencia-Bedregal[1] · H. A. Cabrera-Tinoco[1,3] · S. M. Espinoza Suarez[1] · J. Kargin[4] · N. O. Moreno[5] · C. H. W. Barnes[6] · L. De Los Santos Valladares[1,4,6] (iD)

Abstract

Tons of waste is produced during iron steel's industrial production, creating environmental pollution. This work aims to characterize the steel scale formed on the billet surface during the last step of steel production in the SIDERPERU steel plant. Scanning Electron Microscopy (SEM) shows stacked layers one above the other on steel billets scales surface. Energy Dispersive X-ray (EDX) and X-ray Fluorescence (XRF) reveal the high content of Fe and O, with Ca, Si, Mn, and Cr as minority elemental compounds. X-ray Diffraction (XRD) shows FeO, α-Fe_2O_3 and Fe_3O_4 as crystallographic phases. Magnetometry reveals Verwey transition and paramagnetic signals that screen the Morin transition. Mössbauer Spectroscopy at room temperature displays magnetic and non-magnetic parts. The non-magnetic part has the hyperfine parameters corresponding to predominant nonstoichiometric wustite. Octahedral (Fe^{+2}/Fe^{3+}) and tetrahedral Fe^{3+} hyperfine fields of 46.0 and 49.4 T values respectively are associated to nonstoichiometric magnetite and another sextet with a hyperfine field of 52.0 T is related to hematite.

Keywords Steel billet scale · Continuous casting · Iron oxides · Mössbauer spectroscopy

1 Introduction

Steel production generates a tremendous amount of waste, which is no longer utilized stored in dumps for decades and creates pollution to the environment. Therefore, it is not strange that the steel industry contributes to CO_2 emissions [1]. The steel waste generated

✉ L. E. Borja-Castro
  luis.borja@unmsm.edu.pe

✉ L. De Los Santos Valladares
  ld301@cam.ac.uk

Extended author information available on the last page of the article

can be classified as carbon steel and stainless-steel slag depending on the steel products, and according to the steelmaking process as Electric Arc Furnace (EAF) slag, Ladle Furnance (LF) slag and continuous casting residue (Mill Scales) [2]. There are attempts to recycle EAF and LF slag and utilize them in some sectors, such as for roads, pavements and bricks [3]. Mill scales are the metallurgical waste generated by oxidation process on the surface of the metal during the hot rolling process in the steelmaking industry [4, 5] . Annually, more than 13.5 million tons of mill scale waste are generated around the globe [6], which is treated as waste by the steel industry [4], despite of its high content of Fe and iron oxides minerals composition [7]. SIDERPERU is one of the main leading steel companies in Perú. Its capacity production exceeds the 500 kton of steel finished and by-products. Every 40 min, this steel plant generates a particular batch of a certain batch liquid steel containing iron compounds, calcium and magnesium oxides. In one day of production 90 tons of slag is produced and no longer reused. So, it is crucial to recycle it or to reuse it in other industries to reduce their environmental impact. Kargin et al. has developed and reported a cost-efficient method of processing metallurgical rolling mill scales waste to produces hematite and maghemite nanopowders [8]. In this context, we aim is to characterize the mill scales, known as billet scales, formed during the continuous casting process of steelmaking in the SIDERPERU steel plant and report their content of iron-mineral for later recycling.

2 Experimental details

In SiderPeru, steel is obtained via 'secondary production', i.e. by recycling steel scrap in an electric arc furnace (EAF) between 3000 and 5000 °C. The reduction process of the iron-compounds is performed at 1600–1700 °C in a ladle furnace. The liquid steel is then chemically equilibrated only be composed of iron, carbon and some chemical elements such as Mn and Si in minimum concentration. The transformation into billets is made by pouring this liquid into moulds with a sectional square. Each face of this mould is cooled down with water to solidify the liquid steel. Then the cut is made to specific lengths. Throughout reaction with water and air, white spots are formed on the surfaces of the billets which grow until the so-called steel billet scales are formed. These steel billet scales were collected and characterized. The morphology of the samples was inspected through a scanning electron microscope (SEM) Philips XL-30, with a resolution of 10 nm at 30 kV, Voltage range: 0.5 V to 30 kV and magnification of 300,000× adapted with an EDX-OXFORD Xplorer spectrometer for the semiquantitative elemental analysis. An X-ray fluorescence XRF-720 Shimadzu spectrometer was also used to detect and register the elemental composition, which counts with an advantage algorithm that allows the analysis of a variety of types of matrices.

The X-ray diffraction (XRD) measurements were performed on Rigaku Brand diffractometers using both, cobalt (Co $\lambda_{K\alpha} = 1.79026$ Å) and copper (Cu $\lambda_{K\alpha} = 1.54056$ Å) radiations, in the same geometry conditions. These measures were carried out in order to identify the crystallographic phases present in the sample and to improve the detection of iron oxides detected by copper radiation. The magnetic measurements were carried out using a DC-MPMS-SQUID magnetometer (Quantum Design Inc.) in zero-field cooling (ZFC) and field cooling (FC) modes. The magnetization as a function of temperature was collected from 5 to 400 K and applying an external magnetic field of 500 Oe and 10 kOe. The applied field dependence of the magnetization was also measured in the range ± 10 kOe

and at 5300 and 400 K. The Mössbauer measurement was carried out at room temperature using a Mössbauer spectrometer in transmission geometry. A radioactive source of 57Co (Rh) of 50 mCi of nominal activity was employed with a transducer in constant acceleration with data acquisition in 1024 channels platform. For standard calibration α-Fe foil piece was used and fitting with Lorentzian profiles using the WinNormos software acquired by the laboratory.

3 Results and discussion

Figure 1a) shows a photography taken during the continuous casting of the billets on whose surface scales grow. Figure 1b) shows billets scales formed. They consist of dark gray plate pieces, with smooth surfaces and very brittle to touch by hands. The SEM Micrography with the topography surface and colored map are indicated in Figs. 1c) and d), respectively where it is observed that the scales surface is formed by stackings layers and agglomerated particles of about 100 μm diameters. EDX and XRF spectra in Fig. 1e) and f) show Fe and Ca as common chemical elements. Table 1 lists the elemental composition of the steel billet scales sample. Fe is the main chemical element detected by EDX and XRF techniques. O is the secondary chemical element detected by EDX technique, while Si, Mn, Ca and Co are the minimal elements registered by the same technique. Mn, Cr and Cu detected by XRF also in minimal concentration. The difference in the elemental composition provided by both techniques is mainly related to the difference between penetration depth than inhomogeneity of the sample. To note, XRF penetrates the sample deeper than EDX, allowing the former technique to detect more elements than the second one [9].

Figure 2 shows the obtained result for X-ray Diffraction for steel billet scales. A cobalt target was also used in the measurements to avoid the fluorescence effect by copper radiation in iron oxide components resulting in lower diffraction intensity. For steel billet scale sample, the resultant diffractograms in cobalt and copper radiation are differentiated by their intensity and shape profile, as we can observe for reflections for (111), (200) and (220); (220), (311), (400) and (400); (012), (104), (110), (113), (024), (116) and (300) display in Fig. 2a). The main crystalline phases identified are wüstite (FeO, PDF card No. 01–073-2145). Magnetite (Fe_3O_4, PDF card No. 01–073-2145) is detected as secondary phase, whereas hematite (α-Fe_2O_3. PDF card No. 00–033-0664) appears as minor phase. These components come from the oxidation of iron in contact with water and air during the cooling process of the steel billets. In other words, the oxidation process occurs due to the reaction of Fe with O to form wustite on the surface of the billets. Some proportion of this wustite oxidizes to magnetite and, eventually, as the cooling process reaches the room temperature to hematite [10]. Its related parameters are listed in Table 2. These results obtained by XRD are similar to the reported by Bagatini et al. in their studies on mill scale and Farahat et al. in their work in the reduction of mill scale [11, 12]. Note that the mineral phases are in well agree to compositional elements found by EDX and XRF. Also, in Fig. 2a) and b) we can see a broad peak labeled by in the red square that can be associated with the presence of some iron silicates or carbonate silicates as shown in the EDX and FRX techniques.

Figure 3(a) shows the magnetization as a function of temperature curves of billet scales measured under applied magnetic fields of 500 Oe and 10 kOe. The M(T) curves show a reduction of irreversibility in ZFC and FC over the entire range of temperature as the external field increases from 500 Oe to 10 kOe. This reduction is due to the alignment of
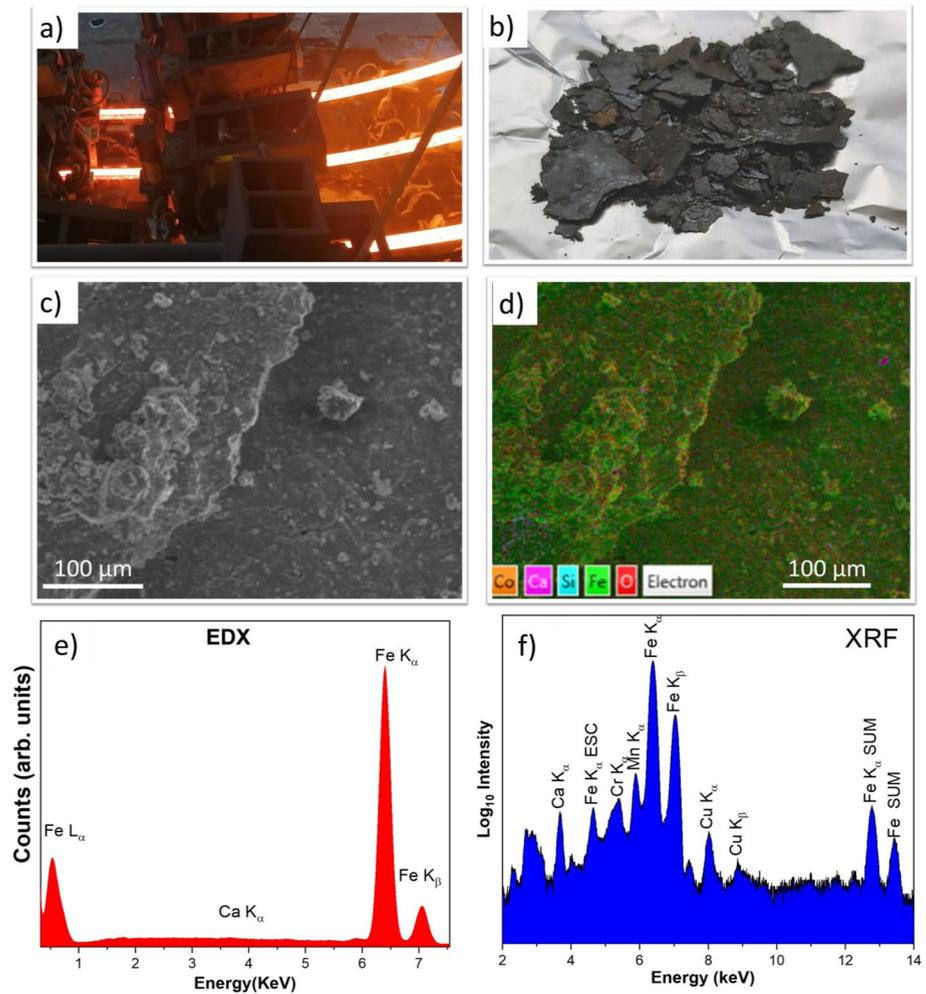
Fig. 1 **a** A photography taken during continuous casting of steel billets where scales are formed, **b** a photography of the scales, **c** and **d** SEM micrograph of scales surface, **e** EDX and **f** XRF spectra

Table 1 Elemental composition for steel billet scale sample

EDX							
Element	Fe	O	Mn	Co	Cu	Si	Ca
Wt%	72.8(1)	25.2(3)	0.78(1)	0.43(2)	0.39(1)	0.25(2)	0.12(1)
XRF							
Element	Fe	–	Mn	–	Cu	–	Ca
Mass %	97.92(1)	–	1.014(1)	–	0.454(1)	–	0.373(2)
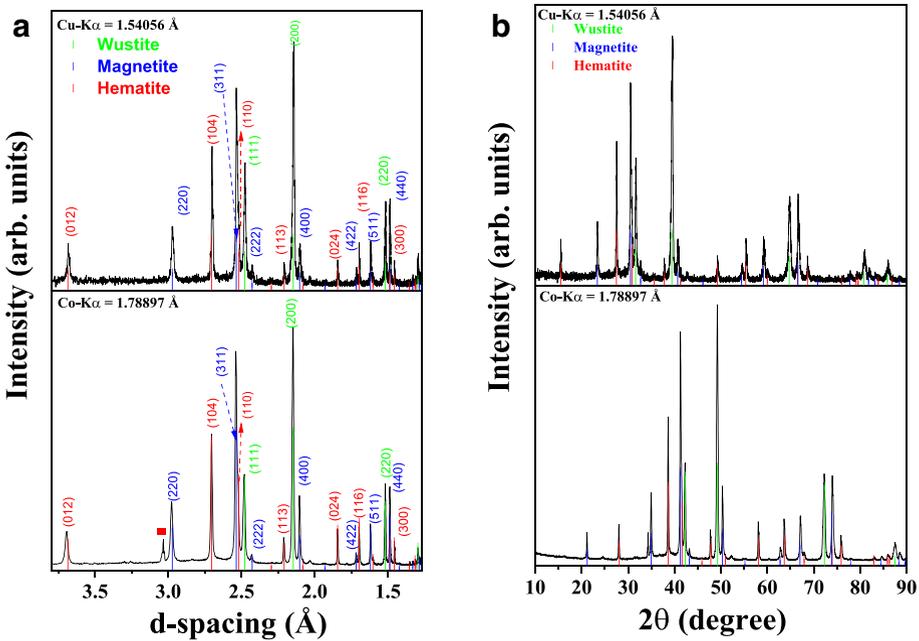
Fig. 2 XRD of steel billet scales collected from SIDERPERU steel plant **a** intensity vs interplanar distance and **b** intensity vs 2θ

ferromagnetic domains to the external field resulting in magnetization gain. Verwey transition [13] is registered at T ~ 120 K when the applied magnetic field is 500 Oe confirming the presence of magnetite detected by XRD. Note that also hematite and wustite were detected by XRD. However, the Morin transition from hematite at 250–260 K [14] and the antiferromagnetic-to-paramagnetic transition of wustite at 200–210 K are not revealed in the M(T) curves. These transitions must be screened by the ferrimagnetic signal of magnetite and signals from other magnetic elements. In this way, under higher applied magnetic fields, such as 10 kOe (blue curve in the figure), most of the domains in the sample align ferromagnetically in the whole range of temperature.

Figure 3(b) displays the external field dependence of the magnetization M(H) at 5, 150, 300 and 400 K. M(H) reveals narrow hysteretic behaviors of soft ferromagnetic materials. From the M–H plots it can be observed that the steel billet scales almost saturated above 9 kOe for all temperatures demonstrating the ferromagnetic alignment. The Mr./Ms. rates values and coercive field tend to decrease with increasing the temperature due to the competition between the thermal and magnetic energy of magnetic domains, as mentioned above. Note that the ratio of Mr./Ms. is by far less than 1, so the bill scale tends to behave more paramagnetic than ferromagnetic.

Figure 4 shows the Mossbauer spectrum taken at room temperature for the scales sample. The hyperfine parameters are listed in Table 3. The spectra are composed of nonmagnetic and magnetic parts. Three Zeeman sextets and two paramagnetic doublets were used to fit the spectra. Two doublets in the fitted spectra correspond to nonstoichiometric wustite ($Fe_{1-x}O$). One doublet is present with $\delta_{Fe} = 0.9$ mm/s and $\Delta E_Q = 0.73$ mm/s due to the electronic exchange between Fe^{2+} and Fe^{3+} in the octahedral site. Another doublet with $\delta_{Fe} = 0.38$ mm/s and $\Delta E_Q = 0.60$ mm/s is attributed to the electronic exchange between

Table 2 Mineralogical phases, relative percentage abundance, cell parameters, Miller indexes, peak positions and crystallite sizes obtained from the XRD analysis of steel billet scale samples

Phase	%	Cell parameters	Miller Index (*hkl*)	2θ (°)	Crystallite size (nm)
Wustite	38.8	a = b = c = 4.288(1) Å; α = β = γ = 90.0 Space: Fm-3 m	111	42.3	56
			200	49.2	32
			220	72.2	23
			311	87.5	22
Magnetite	36.1	a = b = c = 8.395(3) Å.; α = β = γ = 90.0 Space: Fd-3 m	111	21.1	56
			220	34.9	43
			311	41.2	43
			222	43.1	28
			400	50.4	40
			422	62.8	27
			333	67.2	28
			440	74.0	28
			620	84.7	27
			533	88.6	24
Hematite	25.0	a = b = 5.033(3) Å. c = 13.753(4) Å. α = β = 90.0 γ = 120.0 Space: R − 3 c	012	28.0	52
			104	38.6	49
			110	41.5	40
			113	47.8	43
			024	58.1	39
			116	63.7	35
			300	75.9	32
			208	84.7	27
			1010	85.9	59
			119	86.2	23
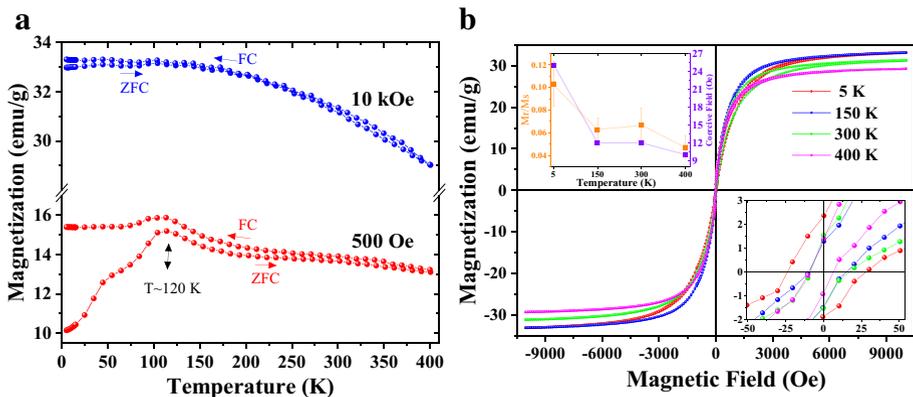
Fig. 3 Magnetic responses of steel billet scales collected from SIDERPERU **a** M(T) at 500 and 10 KOe and **b** M(H), Mr./Ms. rate and coercive fields as insets

Fig. 4 Mössbauer spectrum of billet scales sample from SIDER-PERU steel plant taken at RT
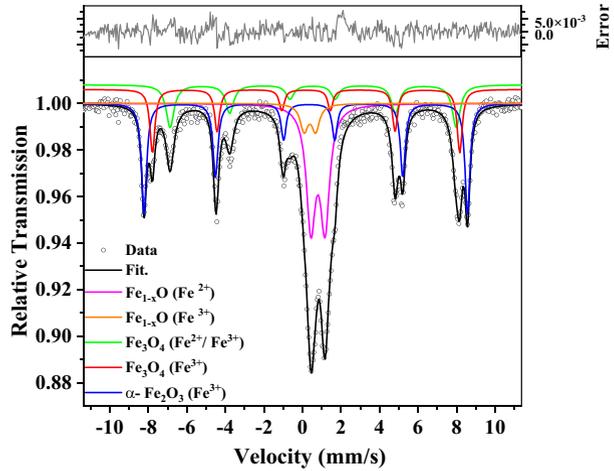
Table 3 Hyperfine parameters values for steel billet scales at room temperature were obtained from Mössbauer spectra fitting. δ_{Fe}: Isomer shift relative to α-Fe at room temperature, ΔE_Q: quadrupole splitting, 2ε: quadrupole splitting, B_{hf} = hyperfine magnetic field, W: line width and RAA: relative absorption area

Subspectra	δ_{Fe} (mm/s)	$\Delta E_Q/2\varepsilon$ (mm/s)	B_{hf} (T)	W (mm/s)	RAA (%)
*Wustite(Fe^{2+})	0.9(2)	0.73(1)	–	0.57(1)	38.9
*Wustite (Fe^{3+})	0.38(3)	0.60(2)	–	0.42(2)	6.1
Magnetite (Fe^{2+}/Fe^{3+})	0.65(2)	0.03(2)	46.0(2)	0.5(2)	20.8
Magnetite (Fe^{3+})	0.30(2)		49.4(3)	0.32	12.8
Hematite	0.36(2)	−0.17(4)	52.0(2)	0.31(4)	21.4

*non-stoichiometric wustite

tetrahedral Fe^{3+} and octahedral Fe^{2+} sites. This result is consistent with the literature [15, 16]. The relative absorption area (RAA) given by the two doublets of wustite accounts for 45% which is in higher proportion. Such results agree with the XRD results suggesting wustite as the main crystallographic phase. Two Zeeman sextets with hyperfine magnetic field B_{hf} = 46.0 and 49.4 T are typical for magnetite in octahedral (Fe^{2+}/Fe^{3+}) and tetrahedral (Fe^{3+}) sites [17, 18], see Table 3. The ratio between the RAA octahedral and tetrahedral sites accounts to 1.63 which is smaller than 1.8 for pure magnetite. This means that the magnetite present in steel billets scales is nonstoichiometric maybe due to the partial substitutions at Fe Sites for the elements registered by EDX and XRF techniques above. Magnetite RAA accounts for 33.6%, thus it is in the intermediate fraction. According to the previous XRD results, the hyperfine magnetic field B_{hf} = 52 T is related to weakly ferromagnetic hematite [19, 20] according to XRD results above.

The relative absorption area obtained from the fitting process of the Mössbauer spectra provides an estimation of the relative abundance of the iron oxide components in the sample. Thus, according to Table 3, wustite in their oxidation states of Fe^{2+} and Fe^{3+} accounts for an RAA ~ 45.0%. The tetrahedral (Fe^{3+}) and octahedral (Fe^{2+}/Fe^{3+}) sites of magnetite give a total RAA of 33.6% and hematite an RAA of 21.4%. These values tell us that most

abundant iron oxide in the sample is wustite, followed by magnetite and hematite. These results agree well agreement with the obtained values by XRD above (see Table 2).

4 Conclusions

Steel billet scales generated during the continuous casting process in SIDERPERU plant were characterized. They have plates in the micrometer scale, that are dark gray in color and very brittle. EDX and XRF found that Fe and O are the main chemical elemental composition. Ca, Si, Mn, Co, Cr were recorded, but in minimal concentration. Wustite (FeO), magnetite (Fe_3O_4) and hematite (α-Fe_2O_3) were found by XRD technique as the main crystallographic phases. Verwey transition signal was detected in the temperature dependent magnetization (M–T) curves at an applied magnetic field of 500 Oe. Above the Verwey temperature the diamagnetic signal of the non-magnetic components screens the Morin transition related to hematite. At 10 kOe a ferromagnetic signal was detected due to the increase of the magnetization values and loss of the ZFC and FC irreversibility. Mössbauer spectroscopy confirms the presence of iron oxides such as wustite, magnetite and hematite. According to the presented results, wustite is the predominant component, magnetite is the intermediate and hematite is the minor one. Mössbauer spectroscopy also has revealed that the wustite and magnetite are non-stoichiometric.

References

1. Pauliuk, S., Milford, R.L., Müller, D.B., Allwood, J.M.: Supplementary information - the steel scrap age. Environ. Sci. Technol. **47**, 3448–3454 (2013)
2. Yi, H., Xu, G., Cheng, H., Wang, J., Wan, Y., Chen, H.: An overview of utilization of steel slag. Procedia Environ. Sci. **16**, 791–801 (2012). https://doi.org/10.1016/j.proenv.2012.10.108
3. Prim, S.R., Folgueras, M.V., de Lima, M.A., Hotza, D.: Synthesis and characterization of hematite pigment obtained from a steel waste industry. J. Hazard. Mater. **192**, 1307–1313 (2011). https://doi.org/10.1016/j.jhazmat.2011.06.034
4. Jikar, P.C., Dhokey, N.B.: Overview on production of reduced iron powder from mill scale waste. Mater. Today Proc. **44**, 4324–4329 (2020). https://doi.org/10.1016/j.matpr.2020.10.552
5. Ruhiyuddin, M.Z., Murizam, D., Ahmad, K.R.: Synthesis and characterization of iron produced from iron mill scale. Key Eng. Mater. **594–595**, 118–122 (2014). https://doi.org/10.4028/www.scientific.net/KEM.594-595.118
6. Cho, S., Lee, J.: Metal recovery from stainless steel mill scale by microwave heating. Met. Mater. Int. **14**, 193–196 (2008). https://doi.org/10.3365/met.mat.2008.04.193

7. Cunha, A.F. da, Mol, M.P.G., Martins, M.E., Assis, P.S.: Caracterização, beneficiamento e reciclagem de carepas geradas em processos siderúrgicos. Rem Rev. Esc. Minas. 59, 111–116 (2006). https://doi.org/10.1590/s0370-44672006000100014
8. Kargin, D.B., Konyukhov, Y.V., Biseken, A.B., Lileev, A.S., Karpenkov, D.Y.: Structure, morphology and magnetic properties of hematite and Maghemite Nanopowders produced from rolling mill scale. Steel Transl. **50**, 151–158 (2020). https://doi.org/10.3103/S0967091220030055
9. Chauhan, A.: Deformation and damage mechanisms of ODS steels under high-temperature cyclic loading. Int. J. Fatigue. **93**, 1–17 (2018)
10. Marciuš, M., Ristić, M., Ivanda, M., Musić, S.: Formation of iron oxides by surface oxidation of iron plate. Croat. Chem. Acta. **85**, 117–122 (2012). https://doi.org/10.5562/cca1943
11. Farahat, R., Eissa, M., Megahed, G.: Reduction of Mill Scale Generated by Steelprocessing. J. Steel Relat. Mater. (2010)
12. Bagatini, M.C., Zymla, V., Osório, E., Vilela, A.C.F.: Characterization and reduction behavior of mill scale. ISIJ Int. **51**, 1072–1079 (2011). https://doi.org/10.2355/isijinternational.51.1072
13. Walz, F.: The Verwey transition - a topical review. J. Phys. Condens. Matter. **14**, (2002). https://doi.org/10.1088/0953-8984/14/12/203
14. Özdemir, Ö., Dunlop, D.J., Berquó, T.S.: Morin transition in hematite: size dependence and thermal hysteresis. Geochemistry, Geophys. Geosystems. **9**, (2008). https://doi.org/10.1029/2008GC002110
15. Gheisari, M., Mozafari, M., Niyaifar, M., Amighian, J., Soleimani, R.: Observation of small exchange bias in defect wüstite (Fe 0.93O) nanoparticles. J. Supercond. Nov. Magn. **26**, 237–242 (2013). https://doi.org/10.1007/s10948-012-1821-9
16. Benard, J.: The oxidation of metals and alloys. Metall. Rev. **9**, 473–503 (1964). https://doi.org/10.1179/mtlr.1964.9.1.473
17. Doriguetto, A.C., Fernandes, N.G., Persiano, A.I.C., Nunes Filho, E., Grenèche, J.M., Fabris, J.D.: Characterization of a natural magnetite. Phys. Chem. Miner. **30**, 249–255 (2003). https://doi.org/10.1007/s00269-003-0310-x
18. Vandenberghe, R.E., De Grave, E.: Application of Mössbauer spectroscopy in earth sciences. Mössbauer Spectrosc. **91–185**, (2013). https://doi.org/10.1007/978-3-642-32220-4_3
19. Gaviría, J.P., Bohé, A., Pasquevich, A., Pasquevich, D.M.: Hematite to magnetite reduction monitored by Mössbauer spectroscopy and X-ray diffraction. Phys. B Condens. Matter. **389**, 198–201 (2007). https://doi.org/10.1016/j.physb.2006.07.056
20. Stevens, J.G., Khasanov, A.M., Miller, J.. W., Pollack, H., Li, Z.: Mössbauer Mineral Handbook. Mössbauer Effect Data Center, The University of North Carolina at Asheville 206 Rhoades Hall (2006)

Authors and Affiliations

L. E. Borja-Castro[1] · A. Bustamante Dominguez[1] · M. I. Valerio-Cuadros[1,2] · R. A. Valencia-Bedregal[1] · H. A. Cabrera-Tinoco[1,3] · S. M. Espinoza Suarez[1] · J. Kargin[4] · N. O. Moreno[5] · C. H. W. Barnes[6] · L. De Los Santos Valladares[1,4,6]

[1] Laboratorio de Cerámicos y Nanomateriales, Facultad de Ciencias Físicas, Universidad Nacional Mayor de San Marcos, Ap. Postal 14-0149, Lima, Peru

[2] Departamento de Física, Universidade Estadual de Maringá, Av. Colombo, 5790 - Jardim Universitário, Maringá, PR 87020-900, Brazil

[3] Facultad de Ingeniería, Universidad Continental, 15311 Lima, Peru

[4] Department of Technologies Commercialization, L. N. Gumilyov Eurasian National University, Astana 010000, Kazakhstan

[5] Departamento de Física, Universidade Federal de Sergipe, São Cristóvão, SE 49100-000, Brazil

[6] Cavendish Laboratory, Department of Physics, University of Cambridge, J.J Thomson Av., Cambridge CB03 0H3, UK